This is the author's version of an article published in ISA Transactions. Changes were made to this version by the publisher prior to publication. DOI: https://doi.org/10.1016/j.isatra.2015.10.022

RTDS Implementation of an Improved Sliding Mode Based Inverter Controller for PV System

Gazi Islam[a], S.M. Muyeen [a], Ahmed Al-Durra [a], Hany M. Hasanien [b]

[a] The Petroleum Institute, Electrical Engineering Department, PO Box 2533, Abu Dhabi, UAE

[b] Electrical Power & Machines Department, Faculty of Engineering, Ain Shams University, Egypt

Abstract

This paper proposes a novel approach for testing dynamics and control aspects of a large scale photovoltaic (PV) system in real time along with resolving design hindrances of controller parameters using Real Time Digital Simulator (RTDS). In general, the harmonic profile of a fast controller has wide distribution due to the large bandwidth of the controller. The major contribution of this paper is that the proposed control strategy gives an improved voltage harmonic profile and distribute it more around the switching frequency along with fast transient response; filter design, thus, becomes easier. The implementation of a control strategy with high bandwidth in small time steps of Real Time Digital Simulator (RTDS) is not straight forward. This paper shows a good methodology for the practitioners to implement such control scheme in RTDS. As a part of the industrial process, the controller parameters are optimized using particle swarm optimization (PSO) technique to improve the low voltage ride through (LVRT) performance under network disturbance. The response surface methodology (RSM) is well adapted to build analytical models for recovery time (R_t), maximum percentage overshoot (MPOS), settling time (T_s), and steady state error (E_{ss}) of the voltage profile immediate after inverter under disturbance. A systematic approach of controller parameter optimization is detailed. The transient performance of the PSO based optimization method applied to the proposed sliding mode controlled PV inverter is compared with the results from genetic algorithm (GA) based optimization technique. The reported real time implementation challenges and controller optimization procedure are applicable to other control applications in the field of renewable and distributed generation systems.

Index Terms—*Current control scheme, DC-AC power converter, DC-DC power converter, parameter optimization, low voltage ride through, power system transients, photovoltaic system, sliding mode controller.*

1. Introduction

The major challenges of grid integrated renewable energy sources like wind and PV are their stability, reliability, and control aspects. The net contribution of electricity from alternative energy sources to some of the major power grids around the world has reached a stage where further integration of those unpredictable energy sources may cause system instability anytime [1]. Political vision of some of these countries in generating a certain proportion of electricity from renewable energy sources also poses a major technological challenge. With the increase in penetration level of renewable sources to the power systems, voltage control by these grid connected energy sources becomes more and more important. For example, during the post fault condition, the terminal voltage must recovers 90% of its nominal value within 1.5 seconds from the fault clearance [2]. Therefore, the inverter control has to be robust enough to handle large scale grid disturbances in order to fulfill the grid code requirements. Sliding mode control is becoming popular method for power electronics inverter control due to its large disturbance rejection capability and less dependency on system parameters variation [3]. Different sliding mode controllers have been used for inverter control as reported in [3-9]. However, for practical implementation, a few issues are very important to be addressed as discussed below.

The first focus should be the testing of the developed sliding mode controller in real time environment as the inverter is equipped with fast-switching power electronics devices. Off-line simulator neither guarantees to meet real time performance constraints using a sampled time embedded computer, especially when the power system is very large, nor can validate the implementation of the controller on power hardware. Therefore, Real Time Digital Simulators (RTDSs) are getting popular nowadays in many fields of electrical engineering. RTDS is developed based upon the state of art advanced parallel processing architecture using Digital Signal Processors (DSP) in order to have reduced computation burden in real time operation. The RTDS hardware interacts with its built-in software during run time and thus performs all the computations in real time. Therefore, RTDS can play an important role in the design and development of large industrial plant or in analyzing exact behavior of complicated nonlinear systems [10-12].

The power system itself is nonlinear in nature, therefore, another focus should be in design optimization of controller parameters to confirm whether it can handle the system uncertainties or not. There are some optimization algorithms which can be applied to tune the controller parameters. Genetic Algorithm is a well-know optimization technique used in many areas including power system. The particle swarm optimization (PSO) is a powerful evolutionary computational technique presented by Eberhart and Kennedy [13, 14] in 1995 and this can be used to get optimal solution in some power system applications

where analytical method doesn't converge. Some other optimization techniques such as harmony search method, bacteria foraging technique, Taguchi approach are also be useful in solving power system optimization problems.

Considering the aforementioned issues, this paper aims at developing and testing sliding mode based inverter for grid-connected PV system in real time environment using RTDS. In the authors' earlier work, sliding mode based inverter controllers were developed which give a good dynamic and transient performance [6, 7]. But their output voltage harmonic profiles are continuous because of using hysteresis buffer as band width limiter. In this paper, delta modulation technique is adopted with sliding mode based inverter control to limit the switching frequency, consequently improved harmonic profile is achieved. As the controller development was explained in details in earlier attempts, this study focuses on the real time implementation of sliding mode controller in RTDS using RSCAD software including the delta modulation scheme. Issues such as parameter setting for the switching devices, frequency response of the system, delays in the control signals etc. are addressed with attention.

Another novel feature of this study is to develop a systematic procedure to obtain the optimized parameters for the proposed sliding mode controlled PV inverter using the response surface methodology (RSM) and PSO techniques. The RSM-PSO based technique is examined as the power system is quite non-linear in nature and it is difficult to express using a suitable transfer function. The optimization performance under a network disturbance is validated with the well-known genetic algorithm (GA) based optimization technique. Low voltage ride through (LVRT) performance and frequency analysis results for the optimized sliding mode based proposed controller is compared with some earlier published works, all in RTDS/RSCAD environment. Although the proposed optimization technique is applied to grid-tied PV inverter, the same procedure can be applied to other renewable energy applications.

2. RTDS- Hardware and Software

Real Time Digital Simulator (RTDS) used in this study is based upon the combination of advanced computer hardware and widespread software [15]. It is featured with parallel processing architecture hardware assembled in hardware modules. Each module consists of processor and communication cards which are connected to each other through a common communication backplane. Processing cards are known as Triple Processor Card (3PC), RISC Processor Card (RPC), Gigabyte Processor Card (GPC), and PB5 which operates upto 1.7 GHz and make it possible to simulate the system at lower than 3 μsec. RTDS also has optical analog to digital converter (OADC) card, Giga Transceiver analog output (GTAO) card, etc., to interface with heal hardware.

The RTDS has a built-in graphical user interface known as RSCAD which can be used to simulate components and control as well as allowing interfacing with hardware. It allows to simulate the system using both large time step and small time step approaches. The power systems components and most of the control blocks are available in the large time step library. The power electronics components are designed for small time step that allows for lower than 3 μsec processing time step. RTDS environment and data flow is shown schematically in Fig. 1. RTDS can be used to validate the performance of any control strategy applied to a certain device in real time before hardware implementation.

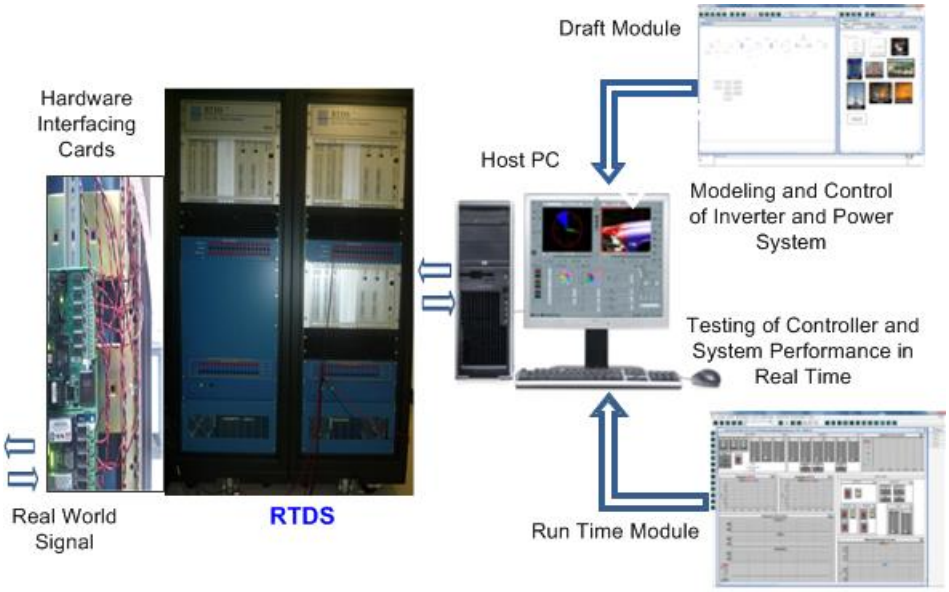

Fig. 1. RTDS working environment

3. Simulated Model System in RTDS/RSCAD

Figure 2(a) shows the schematic diagram of the model system used in this study; the size of the PV plant is 5 MW. A DC-DC boost converter is used for maximum power point tracking. A three-phase voltage source inverter with a delta-wye type transformer is used for grid integration. A double-circuit transmission line is used for connecting the system with power grid. As reported in Sect. 2, RTDS allows simulation in both large and small time step ranges. However, in this work, dual time step approach is considered in simulating the model system to utilize the processors of RTDS in an efficient way as reported in [15, 16]. An interfacing transformer is required to interface large and small time step circuits.

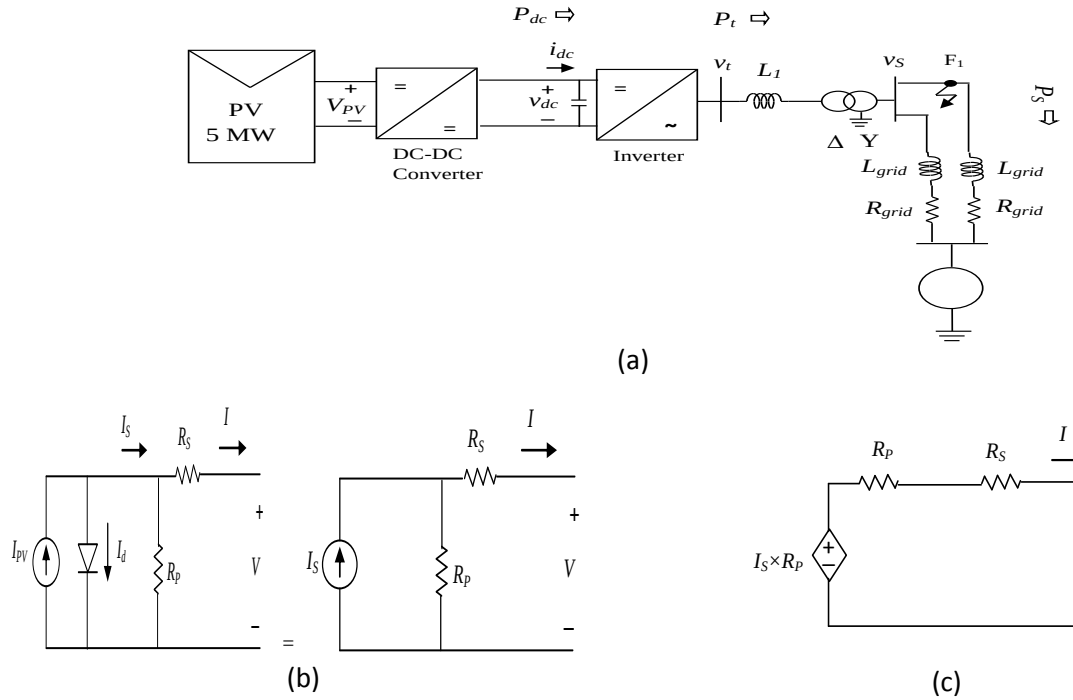

Fig. 2. System Modeling (a) Schematic diagram of the model system (b) Equivalent model of a PV module with current source (c) Modified equivalent model of a PV module with voltage source

An accurate modeling of megawatt class large scale PV system simulated using PSCAD software has been discussed in details in [17]. The same model is used here with multi-string topology for RTDS/RSCAD implementation. The voltage-current (*V-I*) characteristics for a large PV system can be expressed by the following equation:

$$I = \underbrace{N_P I_{PV} - \underbrace{N_P I_0 \left[\exp\left(\frac{q\left(V+IR_{S_{eq}}\right)}{N_M N_S akT}\right) - 1\right]}_{I_d} - \frac{V+IR_{S_{eq}}}{R_{P_{eq}}}}_{I_S} \quad (1)$$

where N_P is the total number of parallel PV strings of the plant, N_M is the number of series modules per string, N_S is the number of series connected cells per module, q is the electron charge; I_o and I_{PV} are reverse saturation current and photo-current of individual modules, R_{Seq} and R_{Peq} are equivalent series and parallel resistances, respectively.

The equivalent circuit for the PV plant from (1) is shown in Fig. 2(b). If the PV plant is modeled in large time step, this will require interfacing transformer to integrate this DC power circuit with the small time step power electronic circuit. With the DC power, the interfacing transformer may not work accurately. Therefore, it is more accurate approach to model the PV system in the small time step. However, the small time step does not have dependent current source model. Therefore, equivalent voltage source should be used to model the PV system in small time step; the modified equivalent circuit with

voltage source is shown in Fig. 2(c). A capacitor is also used in parallel at the output terminals to remove the oscillation of the output at the current source operating zone of the PV plant.

4. Control Implementation in RTDS/RSCAD

4.1. DC-DC Converter Control

DC-DC converter is used for maximum power point tracking (MPPT). For boost converter, the duty ratio (D) is measured from the following equation [18]:

$$\frac{V_O}{V_{in}} = \frac{1}{1-D} \quad (2)$$

where V_O and V_{in} are output and input side voltage of the converter. The error signal between the measured and reference duty ratio is progressed through the PI controller. The constant output voltage (V_O) is maintained by inverter controller. Thus the duty ratio of the DC-DC converter is varied to regulate the input side voltage (V_{in}) in such a way that the output power from the PV plant is maximum. The reference duty ratio is obtained by measuring the open circuit voltage of a pilot module [15, 17].

4.2. Modified Sliding Mode based Inverter Control

The grid side inverter, in general, is controlled through cascaded loops to regulate real and reactive power delivery. In outer loops two PI controllers are used to control the DC link voltage (v_{dc}) and grid side RMS voltage (v_S), and generate reference d and q axis currents for the inner loops, respectively. The error signals between the measured values of DC link voltage and grid side RMS voltage, and their corresponding reference values (v_{dc}^*, and v_S^* respectively) are progressed through the PI controllers; the outputs of the outer loops give the reference currents for the inner loops. The outer loop control scheme can be mathematically expressed as follows:

$$i_d^* = (K_{P\_Vdc} + \frac{K_{I\_Vdc}}{s})(v_{dc}^* - v_{dc}) \quad (3)$$

$$i_q^* = (K_{P\_VS} + \frac{K_{I\_VS}}{s})(v_S^* - v_S) \quad (4)$$

where K_{P_Vdc}, K_{I_Vdc}, K_{P_VS}, and K_{I_VS} are the controller gains. These reference currents are converted from d-q frame to abc frame for the inner current control loops. Sliding mode control has been implemented for current control loops where line current errors are considered as sliding surfaces. Hence, the sliding surfaces are $S_i = i_i^* - i_i$ where subscript i stands for a,b, and c phases. For the inner current control loops, the following control expressions are defined [6, 7]:

$$v_{ti} = K_i sign(S_i) \frac{v_{dc}}{2} \qquad i = a, b, c \qquad (5)$$

where K_i is the sliding mode controller gain. The switching laws are defined as follows:

$U_i > 0$; upper switch is On and lower switch is Off

$U_i < 0$; upper switch is Off and lower switch is On

where $U_i = sign\ (S_i)$. The switching frequency of the above controller will be very high during steady state and the system will become unstable. In [6], a hysteresis buffer is used to limit the frequency. The system gives a very good transient performance. However, terminal voltage has a wide range of frequency spectrum; this makes filter designing a difficult task.

In this study, delta modulation scheme is adopted for sliding mode control. A triangular wave is added to the reference sinusoidal currents. Thus the reference currents become sinusoidal with triangular oscillation and help the measured current to follow it. Therefore, the output voltage will have frequency spectrum predominantly around the frequency of the triangular signal. The complete control block diagram is shown in Fig. 3(a).

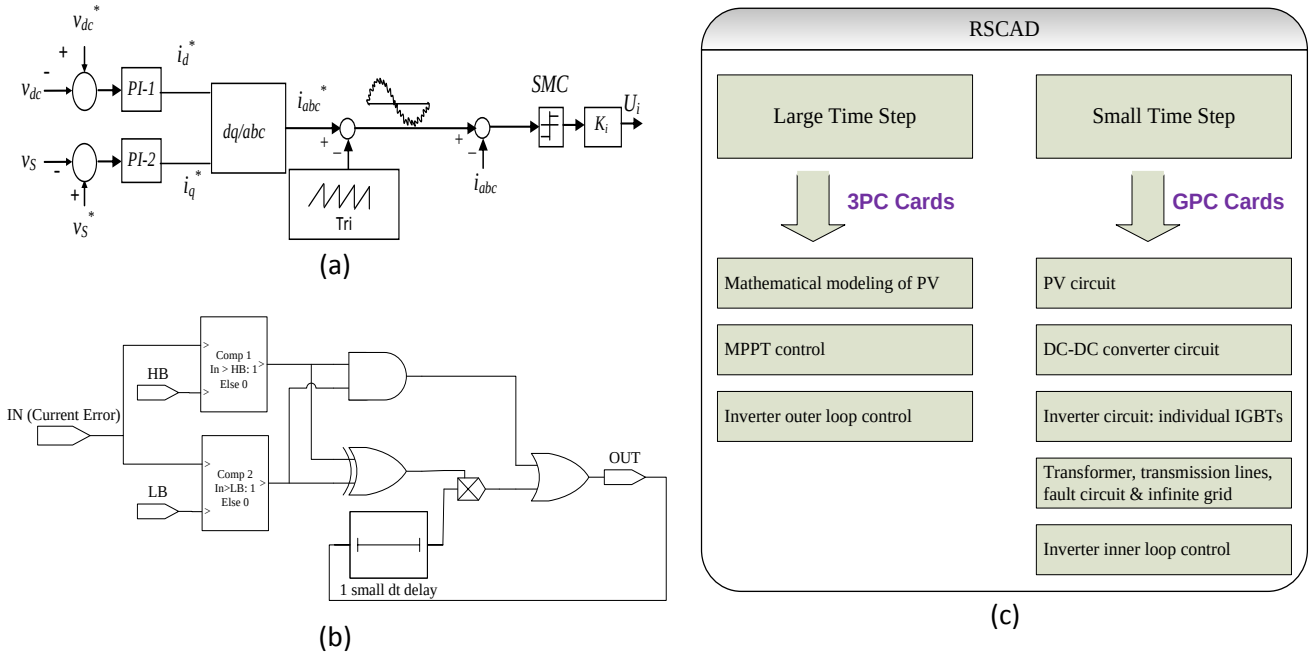

Fig. 3. Real time implementation of PV controller (a) Proposed control scheme (b) Developed hysteresis block in RSCAD (c) RSCAD implementation and processor assignments

5. Challenges of real Time Implementation

5.1. In Terms of Component Modeling

As discussed in Sect. 3, the PV modeling has been done in small time step with equivalent voltage source model. Generally,

the switching circuits are implemented in a small time step whereas the rest of the power circuit is done in a large time step. An interfacing transformer is used to connect small time step circuit to the large time step power system. This set up is perfect for a system that does not need low time step. For example sine triangle modulation technique based PWM converter can be easily implemented with dual time step power circuits. Because RSCAD accommodates at least 17 small time steps followed by a large time step when there is an interfacing transformer in the simulation. RSCAD also sets the small time step size depending on the small time step circuit size. Therefore, simulation time step cannot be set as low as the user want for a particular circuit. On the other hand, it requires a minimum of 7 small time steps only followed by a large time step if the simulation does not have any interfacing transformer. Therefore, user can reduce the overall simulation time step if there is no interfacing transformer. This means, the complete circuit has to be designed in small time step.

For this particular power system, the authors managed to set minimum simulation time step as of 50 µsec when there is an interfacing transformer. For a good dynamic and transient performance of this proposed control system, the simulation time step needs to be much lower than 50 µsec as the bandwidth of the control scheme is high. Therefore, the complete circuit has been remodeled in the small time step. The three-phase inverter is built using individual IGBTs, as gate pulses are generated for individual switches instead of the built in firing pulse generator block from the small time step library, which is suitable for sine triangle modulation based PWM technique. For dynamic analysis, the minimum simulation time step which has been achieved is 17 µsec. However, the small time step library does not have built in tools for fault analysis. Therefore, breakers have been used to introduce faults. Because of these additional components, the minimum allowable simulation time step for transient analysis is found to be 23 µsec.

5.2. In Terms of Control Application

The complete control block for MPPT is designed in large time step as large simulation time step is low enough to work for the low switching frequency of the DC-DC converter. For accurate results, it is important to generate the firing pulses (and inner current control loop) in small time step. In earlier versions of RSCAD, control blocks in small time steps were suitable only for firing pulse generation of sine triangle based PWM schemes only. Newer versions of RSCAD (version 3.0 and higher) have extra control blocks like adder, comparator, logic circuits etc. which can be used for the implementation of the inner control loop in small time step.

It is not the scope of this paper to compare the dynamic and transient performance of the proposed control scheme with that of the controller used in [6] with hysteresis buffer. However, the controller discussed in [6] is also implemented in RSCAD

to validate the frequency distribution of the output voltage. The hysteresis buffer block is not available in small time step. Therefore, the block is developed using the logic circuit shown in Fig. 3(b). The bandwidth (HB and LB in Fig. 3(b)) for this study is chosen to be ±0.08.

The triangle wave for the proposed controller is generated using built-in triangular wave generator block of small time step library. The frequency is 3000 Hz and amplitude is 0.1. System implementation and processor assignment details in RSCAD are shown in Fig. 3(c).

6. Design Optimization of Controller Parameters

The objective is to find the optimum values of two PI controllers used in the sliding mode based PV inverter control shown in Fig. 3(a) to improve the low voltage ride through (LVRT) performance. The following section describes the optimization procedure step by step.

6.1. RSM

Recently, the RSM has received a great potential for modeling, analyzing, and optimizing the design of many electromagnetic devices. This method is a powerful statistical tool used to build an empirical model by finding the relationship between the design variables and response through statistical fitting method [20, 21, 25].In this study, the system analysis on RTDS is used as numerical simulations to provide the response [15]. The recovery time (R_t), maximum percentage overshoot (MPOS), settling time (T_s), and steady state error (E_{ss}) of the voltage profile immediate after inverter are considered in building the analytical models. Those are changed by the design variables variant. The second order model of the RSM is used in this study for obtaining more accurate response. The creation of response surface is based on the central composite design (CCD) which has been widely used for fitting the second order response surface [25].

6.2. PSO Algorithm

The PSO is inspired by the social behavior of bird flocking and fish schooling. It uses a “population” of particles that fly through the problem hyperspace with given velocities. In each iteration, the velocities of the individual particles are stochastically adjusted according to the historical best position for the particle itself and the neighborhood best position. Both the particle and the neighborhood best positions are derived according to a user defined fitness function [14, 22]. The

movement of each particle naturally evolves to an optimal solution. The word "swarm" comes from the irregular movements of the particles in the problem space [22]. The PSO is not affected by the size and nonlinearity of the optimization problem, and can converge to the optimal solution in many problems where most analytical methods fail to converge [23]. The PSO has many merits over other optimization techniques like: 1) It has low number of parameters to adjust unlike many other evolutionary techniques. 2) It has low computational time. 3) It is a derivative free algorithm. 4) It has the flexibility to combine with other optimization techniques to form hybrid tools. 5) It does not depend on the initial solution to start its iteration process [24]. The PSO technique has been successfully applied to solve many power systems and electric machines optimization problems [25-31].

An optimization problem of N variables is considered. The particles of the swarm are initialized in which each particle is assigned a random position in the N-dimensional hyperspace, such that each particle's position corresponds to a candidate solution. The great merit of the PSO algorithm is its simplicity as it consists of two equations only. Each particle is associated with two vectors, the position and velocity vectors. In N-dimensional search space, $X_i = [x_{i1}, x_{i2}, \ldots, x_{iN}]$ and $V_i = [v_{i1}, v_{i2}, \ldots, v_{iN}]$ are the two vectors associated with each particle. The swarm consists of P particles that proceed through the feasible solution space to explore optimal solutions. Each particle can update its position based on its own best exploration, best swarm overall experience, and its previous velocity vector according to the following model [24]:

$$v_i^{k+1} = \omega v_i^k + c_1 r_1 (pbest_i^k - x_i^k) + c_2 r_2 (gbest^k - x_i^k) \qquad (6)$$

$$x_i^{k+1} = x_i^k + v_i^{k+1} \qquad (7)$$

where c_1 and c_2 are two positive acceleration constants; r_1 and r_2 are two randomly generated numbers with a range of [0, 1]; ω is the inertia weight; $pbest_i^k$ is the best position of particle i achieved based on its own experience; $pbest_i^k = [x_{i1}^{pbest}, x_{i2}^{pbest}, \ldots\ldots\ldots, x_{iN}^{pbest}]$; $gbest^k$ is the best particle position based on overall swarm's experience; $gbest^k = [x_1^{gbest}, x_2^{gbest}, \ldots\ldots, x_N^{gbest}]$; and k is the iteration index.

Small acceleration constants c_1 and c_2 allow the particle to diverge from the target regions and large acceleration constants lead to the sudden movement of particles toward target regions [25]. The usual range of c_1 and c_2 are in between 0 and 2. In this study, constants c_1 and c_2 are both set at 2.

6.3. Optimization Procedure

Figure 4(a) shows the flowchart of the overall design strategy. The design procedure is described as follows:

Step 1) Selection of variables and levels:

The PI controller parameters of the control scheme shown in Fig. 3(a) are considered for the design variables. X_1, X_2, X_3, X_4 are proportional gains and integral time constants for PI-1& PI-2, respectively. Table I shows the design variables and levels.

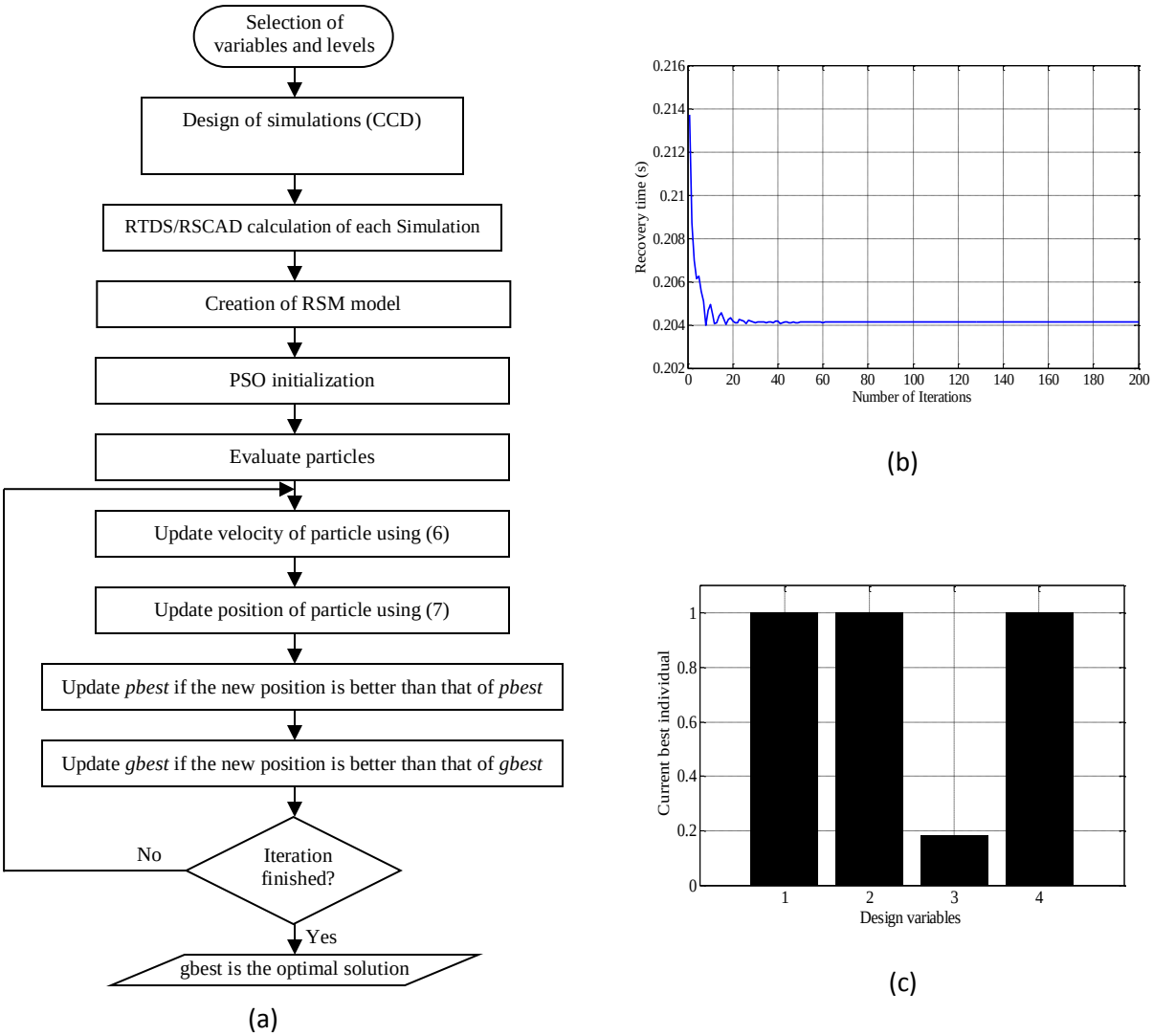

Fig.4. Controller Optimization (a) Flowchart of the proposed PSO approach (b) Recovery time convergence (c) Current best individual.

TABLE I
Design variables and Levels

Design variables Level	*Kp-1* (X_1)	*Ti-1* (X_2)	*Kp-2* (X_3)	*Ti-2* (X_4)
Minimum (-1)	30	20	0.05	0.4
Average (0)	37.5	35	0.075	0.7
Maximum (1)	45	50	0.1	1

Step 2) Design of simulations:

The simulation frequency is set using CCD as shown in Table II. For this study, the frequency of CCD is set to 31 [20, 21, 32].

Step 3) RTDS/RSCAD program calculation:

For each parameter set, simulation is run in real time environment of RTDS/RSCAD in order to calculate R_t, MPOS, T_s and E_{ss}. The results are shown in Table II. As the system is simulated in RTDS/RSCAD environment, 31 scenarios can be obtained in less than 31 minutes, however, offline simulator such as MATLAB/Simulink will take more than 31 hours if the detailed switching model is considered for power electronic inverters.

TABLE II
Range of Design Variables and Experiment Frequency

Exp.	X_1	X_2	X_3	X_4	R_t (Sec)	MPOS (%)	T_s (Sec)	E_{ss} (pu)
1	-1	-1	-1	-1	0.197	10.27	2.67	0.00001
2	1	-1	-1	-1	0.188	9.95	2.73	0.00016
3	-1	1	-1	-1	0.195	10.17	2.74	0.00005
4	1	1	-1	-1	0.196	9.50	2.74	0.0002
5	-1	-1	1	-1	0.195	9.55	2.69	0.0002
6	1	-1	1	-1	0.195	16.04	1.99	0.00039
7	-1	1	1	-1	0.193	9.22	2.75	0.00018
8	1	1	1	-1	0.189	9.00	2.68	0.00022
9	-1	-1	-1	1	0.213	4.47	3.78	0.0029
10	1	-1	-1	1	0.218	4.51	3.44	0.003
11	-1	1	-1	1	0.215	4.53	3.49	0.003
12	1	1	-1	1	0.218	4.65	3.49	0.00255
13	-1	-1	1	1	0.213	4.61	3.68	0.0036
14	1	-1	1	1	0.218	4.36	3.32	0.00286
15	-1	1	1	1	0.215	4.55	3.46	0.0024
16	1	1	1	1	0.217	4.48	3.79	0.0016
17	-1	0	0	0	0.208	5.43	3.42	0.0014
18	1	0	0	0	0.209	5.33	3.44	0.0009
19	0	-1	0	0	0.209	5.40	3.50	0.002
20	0	1	0	0	0.210	5.39	3.60	0.0011
21	0	0	-1	0	0.211	5.56	3.25	0.0016
22	0	0	1	0	0.208	5.38	3.34	0.0012
23	0	0	0	-1	0.186	9.70	2.87	0.00063
24	0	0	0	1	0.219	4.61	3.61	0.003
25	0	0	0	0	0.210	5.30	3.33	0.0036
26	0	0	0	0	0.210	5.30	3.33	0.0036
27	0	0	0	0	0.210	5.30	3.33	0.0036
28	0	0	0	0	0.210	5.30	3.33	0.0036
29	0	0	0	0	0.210	5.30	3.33	0.0036
30	0	0	0	0	0.210	5.30	3.33	0.0036
31	0	0	0	0	0.210	5.30	3.33	0.0036

Step 4) Creation of RSM model:

The four fitted second order RSM model are found as follows:

$$R_t = 0.2098 + 0.003x_1 + 0.0001x_2 - 0.0005x_3 + 0.0117x_4 + 0.0002x_1x_3 + 0.0017x_1x_4 - 0.0008x_2x_3 + 0.0002x_2x_4 + 0.0002x_3x_4 + 0.0001x_1^2 + 0.0005x_2^2 + 0.0009x_3^2 - 0.0064x_4^2 \quad (8)$$

$$MPOS = 5.3 + 0.2789x_1 - 0.4261x_2 + 0.1989x_3 - 2.9239x_4 - 0.425x_1x_2 + 0.4237x_1x_3 - 0.34x_1x_4 - 0.435x_2x_3 + 0.511x_2x_4 - 0.255x_3x_4 + 0.077x_1^2 + 0.092x_2^2 + 0.167x_3^2 + 1.852x_4^2 \quad (9)$$

$$T_s = 3.38 - 0.0589x_1 + 0.0522x_2 - 0.035x_3 + 0.455x_4 + 0.1x_1x_2 - 0.0325x_1x_3 + 0.0212x_1x_4 + 0.072x_2x_3 - 0.051x_2x_4 + 0.051x_3x_4 - 0.206x_1^2 + 0.0994x_2^2 - 0.1556x_3^2 - 0.2106x_4^2 \quad (10)$$

$$E_{ss} = 0.0028 - 0.0001x_1 - 0.0002x_2 + 0.0013x_4 - 0.0001x_1x_3 - 0.0002x_1x_4 - 0.0001x_2x_3 - 0.0002x_2x_4 - 0.0001x_3x_4 - 0.0007x_1^2 - 0.0003x_2^2 - 0.0004x_3^2 \quad (11)$$

The details of the RSM model are discussed in [20, 21, 25, 32].

Step 5) PSO Approach:

The PSO technique is applied to the RSM model. In this paper, MATLAB PSO Toolbox is used [33]. R_t of the voltage profile immediate after inverter is the fitness function, and MPOS, T_s and E_{ss} are considered nonlinear constraint functions. The constraints of the optimized problem are described as follows:

- Design variables range is $30 \leq X_1 \leq 45$, $20 \leq X_2 \leq 50$, $0.05 \leq X_3 \leq 0.1$, and $0.4 \leq X_4 \leq 1$.
- The MPOS constraint $\leq 6\ \%$, T_s constraint $\leq 5\ s$ and E_{ss} constraint ≤ 0.005 p.u.

Table III shows the PSO characteristics, note that the PSO is terminated after 200 iterations. Figure 4(b) shows the recovery time convergence while Table IV shows the optimization set value and level of X_1, X_2, X_3, and X_4. At these optimal values, the recovery time equals 0.2041 s, the MPOS is 6 %, T_s is 3.17 s, and E_{ss} is 0.000796 p.u.

Step 6) GA approach:

For a good comparison, GA technique is also applied to the same optimization problem similar to the PSO approach. MATLAB Optimization Toolbox is also used for this purpose. Table V shows the GA characteristics where after the 50th iterations, the GA optimization was terminated and the average change in the fitness value and the constraint violation were

less than 1e-6. Figure 4(c) shows the current best individual and Table VI shows the optimal level and size value of the design variables. At these optimal values, the R_t equals 0.2178 s, the MPOS is 4 %, T_s is 3.77 s, and E_{ss} is 0.0023 p.u.

TABLE III
PSO Characteristics

PSO Parameters	
Number of particles	50
Initial velocity of the agent	0.0
Acceleration constants	2
Inertia weight	1
No. of iterations	200

TABLE V
GA Characteristics

GA Parameters	
Population type	Double vector
Population size	50
Fitness scaling function	Rank
Selection function	Uniform
Crossover fraction	0.8
Crossover function	Scattered
Migration fraction	0.2
Migration interval	20

TABLE IV
Optimum Level and Size (PSO)

Design variables	X_1	X_2	X_3	X_4
Level				
Optimum level	-1	1	1	-0.42
Optimum size	30	50	0.1	0.57

TABLE VI
Optimum Level and Size (GA)

Design variables	X_1	X_2	X_3	X_4
Level				
Optimum level	1	1	0.18	1
Optimum size	45	50	0.079	1

7. Results and Discussions

The effectiveness of the proposed controller is examined through RTDS/RSCAD simulation in real time environment. The results after adopting proposed parameter optimization technique is compared with some earlier reported results. For smooth understanding, the results are presented in the following sub-sections.

7.1. Frequency Analysis

In authors' earlier work, sliding mode controller in both inner and outer loops were considered [6]. A hysteresis buffer is also considered in that work to limit switching frequency as well as reducing chattering problem and the system was simulated using offline PSCAD/EMTDC software. In this work, the controller is modified and delta modulated sliding mode controller is used in the inner loop only. The proposed controller is implemented in RTDS. Therefore, to make a meaningful comparison, the earlier results shown in [6] is reproduced in RTDS. The frequency spectrum for controller with hysteresis buffer reported in [6] and that of the proposed control scheme are shown in Figs. 5(a) and 5(b), respectively. The frequency distribution shown in Fig. 5(a) is continuous whereas the harmonic spectrum in Fig. 5(b) is similar to that of sine triangle based PWM modulation technique as discussed in Sect. 4.

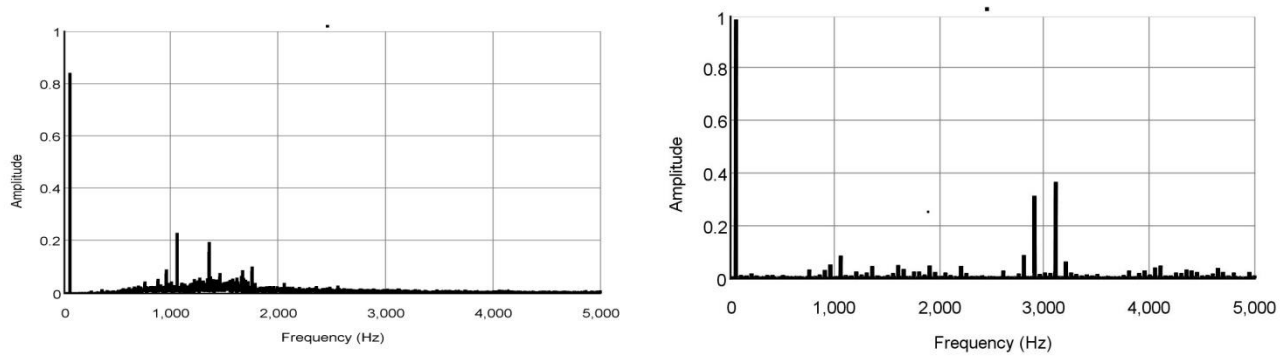

(a) (b)

Fig. 5. Harmonic distribution of grid side voltage for controller with (a) hysteresis buffer (b) proposed controller

7.2. LVRT Analysis

This section is explained into two subsections to demonstrate the effectiveness of the conventional and proposed controllers in order to improve LVRT performance as well as demonstrating the results obtained from the two optimization techniques. For LVRT analysis, a 150 msec fault is considered at F1 location shown in Fig. 2(a). The breaker opened after 0.15 sec and reclosed after 0.8 sec of the starting of fault. It is noted that in real time simulation, it is not possible to set a specific fault time that does in offline simulation as the computation in real time simulator solely depends on the hardware specification and processing power of the simulator.

7.2.1. Case-A:

The proposed controller has inherent characteristics of having overvoltage and under voltage control of inverter DC link. The conventional PI based cascaded controller reported in [6] requires to have over voltage and under voltage control. For the sake of comparison, the conventional controller is simulated in RTDS/RSCAD without having the over voltage and under voltage control. The results obtained from conventional controller of inverter without any over-voltage or under-voltage protection are shown in Fig. 6 for three-line-to-ground-fault (3LG) fault. The controller is unable to limit the overshoot or under-shoot of the DC link voltage which may not allow the PV plant to provide dynamic grid support during severe fault.

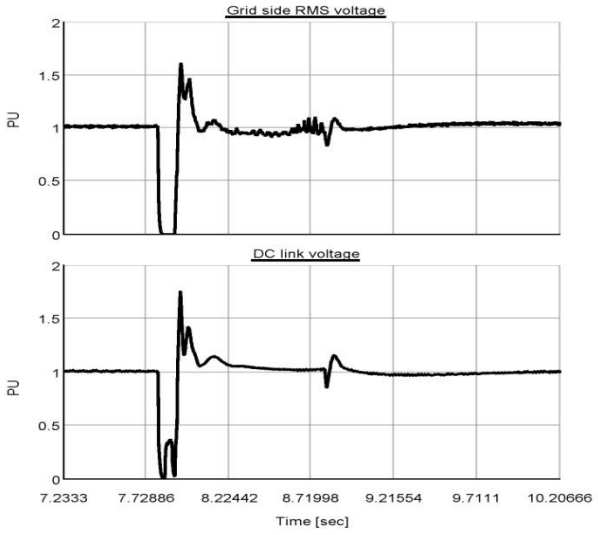

Fig. 6. 3LG fault Responses using conventional controller

The responses of grid side voltage, DC-link voltage, and real and reactive power at the grid end for the proposed controller in case of 3LG fault using the optimum parameters obtained from proposed RSM-PSO technique are shown in Fig. 7. The overshoot for both voltages are less than 10% from the pre-fault values. DC link voltage has no undershoot. Therefore, the controller has inherent under and overvoltage protection which is important for power electronic circuit protection and dynamic grid support. Phase-a current (*ia*) for 3LG fault is also shown with its reference value (*ia**) in Fig. 7. The current closely follows its reference value during steady-state, fault and post-fault conditions. The voltage responses for 2LG and 1LG faults are also shown in Figs. 8(a) and 8(b), respectively using the same optimized parameters obtained from RSM-PSO technique.

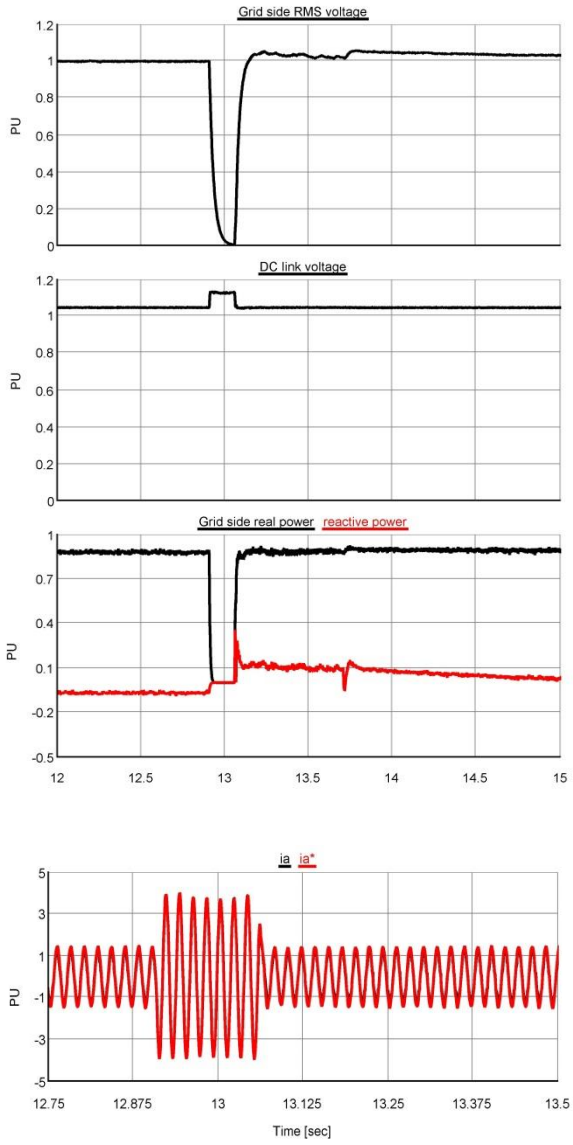

Fig. 7. 3LG fault Responses using the proposed controller with PSO

7.2.2. Case-B:

The LVRT performance of RSM-GA based optimization method is demonstrated in this section. The responses for the grid-side terminal voltage and DC-link voltage for 3LG fault are shown in Fig. 8(c) using the proposed controller. The results in case of 2LG fault using the parameters obtained from RSM-GA are shown in Fig. 8(d). It is seen from Figs. 7, and 8 that though RSM-GA approach has no overshoot, it has higher rise and settling time compared to RSM-PSO based technique. It is noted that the objective of the optimization was to minimize the rise time, R_t. From the simulation results, the rise time, R_t, is found 0.202 sec and 0.22 sec from RSM-PSO and RSM-GA approaches, respectively, in case of 3LG fault.

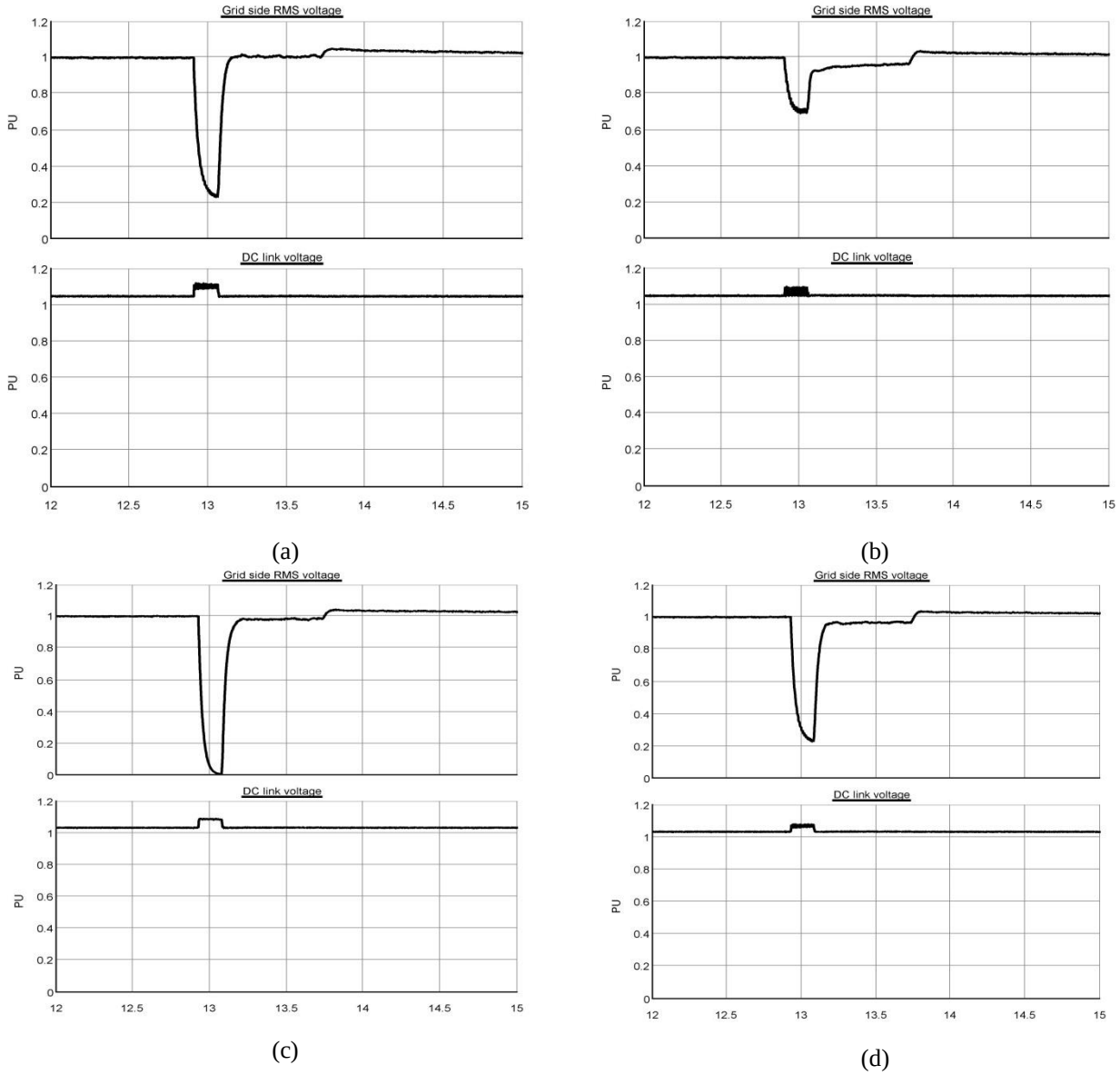

Fig. 8. Other responses using proposed controller with (a) PSO for 2LG (b) PSO for 1LG (c) GA for 3LG (d) GA for 2LG

From the real time simulation results, it is evident that the proposed control strategy exhibits very good transient performance to withstand the low voltage ride through, which is one of the major concerns for grid operators as the grid codes for renewable energy is becoming stringent nowadays. The voltage harmonic distribution also gives a better profile, which was another important objective of the grid tied inverter.

8. Conclusions

This paper has reported a detailed description and technical challenges for real time implementation of a sliding mode based inverter controller for photovoltaic application using Real Time Digital Simulator. The results shows improved performances of the controller during fault conditions. The dynamic performance of the proposed controller is also very good, even though this is not the scope of this work. As a part of the industrial process, the controller optimization process is also emphasized

and a step-by-step optimization procedure is outlined which is very effective for power system application, especially when the system is purely non-linear and difficult to obtain a transfer function. An analytical model for the optimization process is developed based on the response surface methodology. The controller parameters are obtained using two different optimization techniques, PSO, and GA. Finally, the performance of two optimization techniques are examined at grid fault conditions and slightly better performance is obtained from PSO based scheme. The optimization procedure demonstrated in this work can be used in other renewable energy and smart grid applications, distributed generation system, and other power system applications. Thus the proposed control strategy with the optimized parameters would be a good choice for the grid-connected PV system for dynamic conditions as well as for low voltage ride through during severe network faults.

Acknowledgement

This work is financially supported by "The Petroleum Institute Research Center (PIRC)" in Abu Dhabi, UAE.

References

[1] M. Bragard, N. Soltau, S. Thomas, R. Doncker, The Balance of Renewable Sources and User Demands in Grids: Power Electronics for Modular Battery Energy Storage Systems, IEEE Transactions on Power Electronics 25 no. 12 (2010) 3049 – 3056.

[2] Bundesverband der Energie- und Wasserwirtschaft, BDEW., Technical guideline - generating plants connected to the medium-voltage network, (2008).

[3] V. Raviraj, P. Sen, Comparative study of proportional-integral, sliding mode, and fuzzy logic controllers for power converters, IEEE Transactions on Industrial Electronics 33 no. 2 (1997) 518-524.

[4] M. Martinez, A. Susperregui, G. Tapia, L. Xu, Sliding-mode control of a wind turbine-driven double-fed induction generator under non-ideal grid voltages, IET Renewable Power Generation 7 no. 4 (2013) 370 – 379.

[5] L. Jianing, S. Shiping, L. Guiying, Q. Zhiqing, D. Hang, The sliding mode control method of grid-connected inverter applied to three-phase intermittent power supply, Proc. 29th Chinese Control Conference (CCC), Beijing, China, 2010.

[6] G. Islam, A. Al-Durra, S.M. Muyeen, J. Tamura, Performance Analysis of a Sliding Mode Control for Distributed Generations, The 15th International Conference on Electrical Machines and Systems (ICEMS2012), Sapporo, Japan, 2012.

[7] G. Islam, A. Al-Durra, S.M. Muyeen, J. Tamura, A Robust Control Scheme to Enhance the Stability of a Grid-connected Large Scale Photovoltaic System, IEEE PES Transmission and Distribution Conference and Exposition, Florida, USA, 2012.

[8] M. Curkovic, K. Jezernik, and R. Horvat, "PMSM sliding mode FPGA-based control for torque ripple reduction ," IEEE Trans. on Power Electronics, vol. 28, no. 7, pp. : 3549 - 3556, 2013.

[9] M. Curkovic, K. Jezernik, and R. Horvat, "FPGA-Based Predictive Sliding Mode Controller of a Three-Phase Inverter," IEEE Trans. on Industrial Electronics, vol. 60, No. 2, pp. 637-644, 2013.

[10] M. Singh, A. Chandra, Real-Time Implementation of ANFIS Control for Renewable Interfacing Inverter in 3P4W Distribution Network, IEEE Transactions on Industrial Electronics 60 no. 1 (2013) 121-128.

[11] Y. Sekine, K. Takahashi, T. Sakaguchi, Real-time simulation of power system dynamics, International Journal of Electrical Power & Energy Systems 16 no. 3 (1994) 145-156.

[12] M. Faruque, V. Dinavahi, W. Xu, Algorithms for the accounting of multiple switching events in digital simulation of powerelectronic systems, IEEE Transactions on Power Delivery 20 no. 2 (2005) 1157–1167.

[13] J. Kennedy, R. Eberhart, Particle swarm optimization, Proc. IEEE Int. Con. Neural Netw. (ICNN), 1995, pp. 1942-1948.

[14] R. Eberhart, J. Kennedy, A new optimizer using particle swarm theory, Proc. 6th Int. Symp. Micro Machine and Human Science (MHS), 1995, pp. 39–43.

[15] Real Time Digital Simulator Power System and Control User Manual, RTDS Technologies, 2009.

[16] A. Sattar, A. Al-Durra, S.M. Muyeen, Dynamic Characteristics Analysis of Wind Farm Integrated with STATCOM Using RTDS, Proc. 11th International Conference on Electrical Power Quality and Utilisation (EPQU), 2011.

[17] G. Islam, A. Al-Durra, S.M. Muyeen, J. Tamura, Low Voltage Ride Through Capability Enhancement of Grid Connected Large Scale Photovoltaic System, IEEE Annu. Conf. Ind. Electron. Soc. (IECON'11), Melbourne, Australia, 2011.

[18] N. Mohan, T. Undeland, W. Robbins, Power Electronics: Converters, Applications, and Design, Third ed., John Wiley & Sons, 2003.

[19] G. Hart, H. Branz, C. Cox, Experimental tests of open-loop maximum-power-point tracking techniques, Solar Cells 13 (1984) 185-195.

[20] Hany M. Hasanien, A. Abd-Rabou, S. Sakr, Design Optimization of Transverse Flux Linear Motor for Weight Reduction and Performance Improvement Using Response Surface Methodology and Genetic Algorithms, IEEE Transactions on Energy Conversion 25 no. 3 (2010) 598-605.

[21] Hany M. Hasanien, S. M. Muyeen, Design optimization of controller parameters used in variable speed wind energy conversion system by genetic algorithms, IEEE Transactions on Sustainable Energy 3 no. 2 (2012) 200-208.

[22] R. Eberhart, Y. Shi, J. Kennedy, Swarm Intelligence, Morgan Kaufmann, San Mateo, CA, 2001.

[23] Y. Valle, G. Venayagamoorthy, S. Mohagheghi, J. Hernandez, R. Harley, Particle swarm optimization: basic concepts, variants and applications in power systems, IEEE Transactions on Evolutionary Computation 12 no. 2 (2008) 171-195.

[24] M. AlRashidi, M. El-Hawary, A Survey of particle swarm optimization applications in electric power systems, IEEE Transactions on Evolutionary Computation 13 no. 4 (2009) 913-918.

[25] Hany M. Hasanien, Particle swarm design optimization of transverse flux linear motor for weight reduction and improvement of thrust force, IEEE Transactions on Industrial Electronics 58 no. 9 (2011) 4048-4056.

[26] K. Sundareswaran, S. Peddapati, S. Palani, Application of random search method for maximum power point tracking in partially shaded photovoltaic systems, IET Renewable Power Generation 8 no. 6 (2014) 670 – 678.

[27] B. Biswal, P. Dash, B. Panigrahi, Power quality disturbance classification using fuzzy C-means algorithm and adaptive particle swarm optimization, IEEE Transactions on Industrial Electronics 56 no. 1 (2009) 212-220.

[28] C. Liu, Y. Hsu, Design of a self-tuning PI controller for a STATCOM using particle swarm optimization, IEEE Transactions on Industrial Electronics 57, no. 2 (2010) 702-715.

[29] T. Ting, M. Rao, C. Loo, A Novel approach for unit commitment problem via an effective hybrid Particle swarm optimization, IEEE Transactions on Power Systems 21 no. 1 (2006) 411-418.

[30] A. Soroudi, M. Afrasiab, Binary PSO-based dynamic multi-objective model for distributed generation planning under uncertainty, IET Renewable Power Generation 6 no. 2 (2012) 67 – 78.

[31] A. Arkadan, M. ElBsat, M. Mneimneh, Particle swarm design optimization of ALA rotor SynRM for traction applications, IEEE Transactions on Magnetics 45 no. 3 (2009) 956-959.

[32] Raymond H. Myers, Douglas C. Montgomery, and Christine M. Anderson-Cook Response Surface Methodology: Process and Product Optimization Using Designed Experiments, John Wiley & Sons, 3rd Edition,January, 2009

[33] Release 2008a, Particle Swarm Optimization Toolbox, The Math Works press, 2008.